Proceedings of the 2015
IEEE Conference on Robotics and Biomimetics
Zhuhai, China, December 6-9, 2015

Analysis of underwater snake robot locomotion based on a control-oriented model

A. M. Kohl*, K. Y. Pettersen*, E. Kelasidi* and J. T. Gravdahl†

Abstract— **This paper presents an analysis of planar underwater snake robot locomotion in the presence of ocean currents. The robot is assumed to be neutrally buoyant and move fully submerged with a planar sinusoidal gait and limited link angles. As a basis for the analysis, an existing, control-oriented model is further simplified and extended to general sinusoidal gaits. Averaging theory is then employed to derive the averaged velocity dynamics of the underwater snake robot from that model. It is proven that the averaged velocity converges exponentially to an equilibrium, and an analytical expression for calculating the forward velocity of the robot in steady state is derived. A simulation study that validates both the proposed modelling approach and the theoretical results is presented.**

I. Introduction

The development of novel methods in autonomous underwater operations, such as underwater exploration, monitoring, surveillance and inspection, is a research field that is currently receiving a lot of attention. Amphibious and underwater snake robots (USRs) are considered promising to improve the autonomy and efficiency of next generation underwater vehicles for such operations [1,2]. Research on such robots has therefore been increasing recently.

A basis for the development of USRs is provided in the studies of the locomotion mechanisms of both fish [3] and snakes [4]. The first snake prototype for ground applications was presented in [5]. More recently, also prototypes of USRs have been developed [1,6,7] and mathematical models have been presented [1,2,8]. Due to the complexity of the dynamics of a snake robot, all these models have in common that they are highly non-linear. Furthermore, it was shown in [9] that a control law that stabilises snake robot locomotion has to be time-varying. For these reasons, an analysis of snake robot locomotion, as well as motion planning and control design, are very challenging. This problem was approached in [10,11], where a control-oriented model for USRs was developed in order to approach these tasks. Because of the sinusoidal nature of snake locomotion, averaging is an appealing method for its analysis. It has been applied several times in the literature, for example for ground robots [9,12], for fish robots [13], and for USRs [14,15]. In [14], the authors show properties of eel-like motion for a three-linked and a five-linked robot. In [15], the stability of USR locomotion under the influence of both resistive and reactive fluid forces is analysed. However, the fluid is assumed to be steady in all these cases. One important contribution of this paper compared to previous work is the analysis of USR locomotion with an arbitrary number of links under the disturbance of ocean currents.

This paper has several contributions. An existing, control-oriented model [11] is improved by the following simplifications and generalisations: It is argued that the model of forward propulsion can be simplified depending on the fluid drag parameters. In addition, it is shown that a further simplification of the model can be achieved by disregarding added mass effects while still maintaining the same model behaviour. Furthermore, restrictive assumptions that were made on the gait of the USR are relaxed. In particular, the robot is no longer assumed to laterally undulate with a fixed amplitude, but can now move according to a general sinusoidal gait, including eel-like motion. The improved control-oriented model is the basis for the analysis of USR locomotion based on averaging theory. The averaged velocity of the USR is shown to converge exponentially to a steady state velocity, and an analytical expression for the relative forward velocity is presented as a function of the gait parameters. Whereas only few simulation results were presented in [11], this paper presents an extensive simulation study comparing the proposed control-oriented model to a first-principle model as well as validating the theoretical results of the averaging analysis.

The paper is organised as follows. In Sec. II, a control-oriented model of USRs that was derived in [11], based on a first-principle model of USRs from [2], is presented. This model is then further simplified and extended to general sinusoidal gaits. Sec. III presents the control system, which propels the USR. In Sec. IV, the velocity dynamics of the closed-loop system is analysed using averaging theory. Simulation results that validate the theoretical findings are given in Sec. V and conclusions are presented in Sec. VI.

II. A control-oriented model of a USR

This section first summarises a control-oriented model of a USR, that was presented in [11]. In the second part of the section, this model is further simplified by discussing how to approximate the drag force and showing that added mass effects can be disregarded for the studied scenarios. The model is then generalised by relaxing a restrictive assumption on the gait.

*Centre for Autonomous Marine Operations and Systems (AMOS), Department of Engineering Cybernetics at NTNU, NO-7491 Trondheim, Norway. E-mail: {Anna.Kohl,Eleni.Kelasidi,Kristin.Y.Pettersen}@itk.ntnu.no

†Department of Engineering Cybernetics at NTNU, NO-7491 Trondheim, Norway. E-mail: Tommy.Gravdahl@itk.ntnu.no

This work was partly supported by the Research Council of Norway through its Centres of Excellence funding scheme, project no. 223254-AMOS.

978-1-4673-9675-2/15/$31.00 © 2015 IEEE

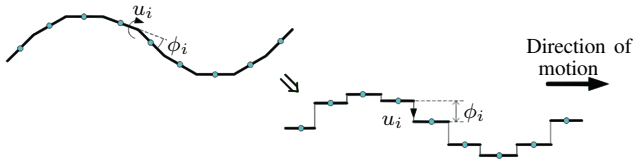

Fig. 1. Modelling of the revolute joints as prismatic joints [16]

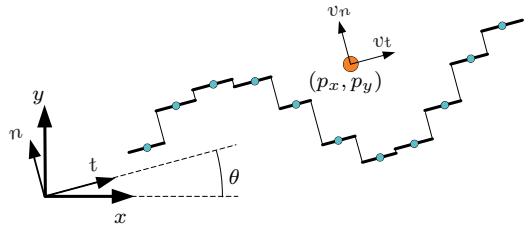

Fig. 2. The control-oriented model [16]

A. Modelling approach

We consider a fully submerged, neutrally buoyant underwater snake robot that conducts a planar, undulating gait with limited link angles and is exposed to an irrotational, constant ocean current. The control-oriented model that will be summarised in the following, was derived in [11]. It was derived from a complex first-principle model in [2], in order to make model-based analysis and control design feasible by the simpler structure. It is based on a simplified kinematic approach, that was first suggested for ground robots in [16] and later for USRs in a resting fluid in [10]: the revolute joints of the snake robot are modelled as prismatic joints, which have a degree of freedom normal to the direction of motion of the robot, as shown in Fig. 1. This approximation is based on the assumption that the single link angles θ_i, and thus also the joint coordinates ϕ_i, are small.

Assumption 1: The link angles satisfy $|\theta_i| < 20°$.

The USR is assumed to undulate in a virtual plane. Since the robot is assumed to be neutrally buoyant, this plane can be any plane in $\mathbb{R}^3$, as pointed out in [17]. The USR consists of N links of length $L = 2l$ and mass m, that are connected by $N-1$ joints, which are modelled to have one translational degree of freedom each. The robot thus has $N+2$ degrees of freedom, two corresponding to the position in the plane, $N-1$ corresponding to the joint coordinates ϕ_i, and one to the orientation θ. The joint coordinates ϕ_i are prismatic and controlled by the input $\mathbf{u} \in \mathbb{R}^{N-1}$. For the mathematical modelling, two coordinate frames are introduced: the global x-y-frame, and the body-aligned t-n-frame that rotates with the robot. The coordinate frames are depicted in Fig. 2.

For describing the system, the state vector $\mathbf{x}$ is defined as

$$\mathbf{x} = [\boldsymbol{\phi}^T \ \theta \ p_x \ p_y \ \mathbf{v}_\phi^T \ v_\theta \ v_t \ v_n]^T \in \mathbb{R}^{2N+4}. \tag{1}$$

The complete control-oriented model is then given by

$$\dot{\boldsymbol{\phi}} = \mathbf{v}_\phi, \tag{2a}$$
$$\dot{\theta} = v_\theta, \tag{2b}$$
$$\dot{p}_x = v_t \cos\theta - v_n \sin\theta, \tag{2c}$$
$$\dot{p}_y = v_t \sin\theta + v_n \cos\theta, \tag{2d}$$
$$\boldsymbol{\mathcal{M}}(\boldsymbol{\phi})\dot{\mathbf{v}}_\phi = -\boldsymbol{\mathcal{D}}(\boldsymbol{\phi})\mathbf{v}_\phi - \boldsymbol{\mathcal{K}}(\boldsymbol{\phi}, \mathbf{v})\boldsymbol{\phi} + \mathbf{D}\mathbf{D}^T\mathbf{u}, \tag{2e}$$
$$\dot{v}_\theta = -\lambda_1 v_\theta + \tfrac{\lambda_2}{N-1} v_{t,\mathrm{rel}} \bar{\mathbf{e}}^T \boldsymbol{\phi}, \tag{2f}$$
$$\dot{v}_t = h_1(\boldsymbol{\phi})\Big[h_2(\boldsymbol{\phi})v_{n,\mathrm{rel}} + h_3(\boldsymbol{\phi})v_{t,\mathrm{rel}} - c_p N\widetilde{m}\boldsymbol{\phi}^T\mathbf{A}\bar{\mathbf{D}}\mathbf{v}_\phi - \mu_p N\widetilde{m}\boldsymbol{\phi}^T\mathbf{A}\bar{\mathbf{D}}\dot{\mathbf{v}}_\phi\Big], \tag{2g}$$
$$\dot{v}_n = h_1(\boldsymbol{\phi})\Big[h_4(\boldsymbol{\phi})v_{n,\mathrm{rel}} + h_5(\boldsymbol{\phi})v_{t,\mathrm{rel}} - 2c_p\mu_p\bar{\mathbf{e}}^T\boldsymbol{\phi}\boldsymbol{\phi}^T\mathbf{A}\bar{\mathbf{D}}\mathbf{v}_\phi - 2\mu_p^2\bar{\mathbf{e}}^T\boldsymbol{\phi}\boldsymbol{\phi}^T\mathbf{A}\bar{\mathbf{D}}\dot{\mathbf{v}}_\phi\Big], \tag{2h}$$

where the matrices $\boldsymbol{\mathcal{M}}(\boldsymbol{\phi}), \boldsymbol{\mathcal{D}}(\boldsymbol{\phi}), \boldsymbol{\mathcal{K}}(\boldsymbol{\phi}, \mathbf{v})$ are

$$\begin{aligned}
\boldsymbol{\mathcal{M}}(\boldsymbol{\phi}) &= \widetilde{m}\mathbf{I}_{N-1} + N\widetilde{m}\mu_p^2 h_1(\boldsymbol{\phi})\mathbf{A}\mathbf{D}^T\boldsymbol{\phi}\boldsymbol{\phi}^T\mathbf{A}\bar{\mathbf{D}}, \\
\boldsymbol{\mathcal{D}}(\boldsymbol{\phi}) &= c_n\mathbf{I}_{N-1} + N\widetilde{m}c_p\mu_p h_1(\boldsymbol{\phi})\mathbf{A}\mathbf{D}^T\boldsymbol{\phi}\boldsymbol{\phi}^T\mathbf{A}\bar{\mathbf{D}}, \\
\boldsymbol{\mathcal{K}}(\boldsymbol{\phi}, \mathbf{v}) &= \mathbf{A}\mathbf{D}^T\big[2N\mu_p h_1(\boldsymbol{\phi})\bar{\mathbf{e}}^T\boldsymbol{\phi}\big(c_n\mu_p - \widetilde{m}c_p\big)v_{n,\mathrm{rel}} \\
&\quad + N\widetilde{m}h_1(\boldsymbol{\phi})\big(N\mu_p c_t + \widehat{c}_n\mu_p\mathbf{e}^T(\mathbf{A}^T\boldsymbol{\phi})^2 - Nmc_p\big)v_{t,\mathrm{rel}}\big].
\end{aligned} \tag{3}$$

The operator $(\cdot)^2$ applied to a vector means that each of the vector's elements is squared. The functions $h_i(\boldsymbol{\phi})$ are

$$\begin{aligned}
h_1(\boldsymbol{\phi}) &= \big[N^2 m\widetilde{m} - 4\mu_p^2(\bar{\mathbf{e}}^T\boldsymbol{\phi})^2\big]^{-1}, \\
h_2(\boldsymbol{\phi}) &= 2N\bar{\mathbf{e}}^T\boldsymbol{\phi}(c_p\widetilde{m} - c_n\mu_p), \\
h_3(\boldsymbol{\phi}) &= \big(4c_p\mu_p(\bar{\mathbf{e}}^T\boldsymbol{\phi})^2 - N^2\widetilde{m}c_t - N\widetilde{m}\widehat{c}_n\mathbf{e}^T(\mathbf{A}^T\boldsymbol{\phi})^2\big), \\
h_4(\boldsymbol{\phi}) &= \big(4c_p\mu_p(\bar{\mathbf{e}}^T\boldsymbol{\phi})^2 - N^2 mc_n\big), \\
h_5(\boldsymbol{\phi}) &= 2\bar{\mathbf{e}}^T\boldsymbol{\phi}\big(Nc_p m - Nc_t\mu_p - \widehat{c}_n\mu_p\mathbf{e}^T(\mathbf{A}^T\boldsymbol{\phi})^2\big).
\end{aligned} \tag{4}$$

In the equations above, $v_{t,\mathrm{rel}}$ and $v_{n,\mathrm{rel}}$ are the relative velocities in the body-aligned frame. They are obtained by

$$\begin{bmatrix} v_{t,\mathrm{rel}} \\ v_{n,\mathrm{rel}} \end{bmatrix} = \begin{bmatrix} v_t \\ v_n \end{bmatrix} - \begin{bmatrix} V_t \\ V_n \end{bmatrix}, \tag{5}$$

where V_t and V_n denote the ocean current velocities in the body-aligned frame. Furthermore, the following matrices and vectors are defined: The unity matrix $\mathbf{I}_N \in \mathbb{R}^{N\times N}$,

$$\mathbf{A} = \begin{bmatrix} 1 & 1 & & \\ & \ddots & \ddots & \\ & & 1 & 1 \end{bmatrix}, \qquad \mathbf{D} = \begin{bmatrix} 1 & -1 & & \\ & \ddots & \ddots & \\ & & 1 & -1 \end{bmatrix},$$

with $\mathbf{A}, \mathbf{D} \in \mathbb{R}^{(N-1)\times N}$. In addition, the summation vectors $\mathbf{e} = \begin{bmatrix} 1 & \dots & 1 \end{bmatrix}^T \in \mathbb{R}^N$, $\bar{\mathbf{e}} = \begin{bmatrix} 1 & \dots & 1 \end{bmatrix}^T \in \mathbb{R}^{N-1}$, and the pseudo-inverse $\bar{\mathbf{D}} = \mathbf{D}^T\left(\mathbf{D}\mathbf{D}^T\right)^{-1} \in \mathbb{R}^{N\times(N-1)}$ are used. Finally, c_n and c_t are the drag parameters in normal and tangential direction, c_p is a propulsion coefficient, λ_i are empirical constants determining the rotational dynamics, μ_p is an added mass parameter, and $\widetilde{m}$ is a generalized mass. The coefficient $\widehat{c}_n$ will be discussed in the next section.

Remark 1: Note that (2) is in closed form. The derivatives in the r.h.s. of (2g, 2h) can easily be eliminated with (2e).

B. Improvements to the model

In the following, at first some further simplifications of the control-oriented model (2) will be presented. Then, the gait of the model will be generalised. The obtained model will serve as the basis for analysing USR locomotion in Sec. IV.

1) Computation of $\widehat{c}_n$: In [11], the coefficient $\widehat{c}_n$ was introduced in order to compensate for model inaccuracies that occurred when there was a large ratio between the drag parameter in normal and tangential direction: $\frac{c_n}{c_t} > 10$. This was based on considerations in [9], where the authors had warned that a large $\frac{c_n}{c_t}$ ratio would lead to inaccuracies, and

TABLE I

RELATIVE VELOCITY WITH AND WITHOUT ADDED MASS EFFECTS

N	$g(i)$	α	ω	δ	rel. error
7	$\frac{N-i}{N+1}$	2.94 cm	120°/s	40°	0.19 %
10	$\frac{N-i}{N+1}$	5.79 cm	120°/s	40°	0.09 %
10	1	5.79 cm	80°/s	40°	4.8e-05 %
19	1	5.33 cm	120°/s	60°	1.8e-05 %

on the assumption that the $\frac{c_n}{c_t}$ ratio would typically be much larger for USRs than for ground snake robots. See [11] for details. However, recent experimental studies suggest that the $\frac{c_n}{c_t}$ ratio is not as large as assumed in [11]. On the contrary, the parameter identification that was presented in [18] showed that the $\frac{c_n}{c_t}$ ratio of the physical robot Mamba [7] is $\frac{c_n}{c_t} \approx 4$, which is close to the ratio of a ground robot $\frac{c_n}{c_t} = 3$ [9], where $\widehat{c}_n$ was not considered: $\widehat{c}_n = 0$. In the remainder of this paper, we will therefore also choose $\widehat{c}_n = 0$, which simplifies the model. We will present simulation results in Sec. V, that show a good accordance between that simplified model and the complex model presented in [2], using the parameters that were identified in [18].

The question of when to include $\widehat{c}_n$ in the modelling remains a trade-off between simplicity and accuracy. It should be kept in mind that setting $\widehat{c}_n$ to zero has the significant advantage of capturing the behaviour of the USR while providing a very simple model. On the other hand, including $\widehat{c}_n$ compensates for an overestimation of the forward velocity, that will occur for a large $\frac{c_n}{c_t}$ ratio.

2) Added mass effects: A common assumption for slow motion of underwater vehicles is to disregard added mass effects. This assumption has often been made for models of USRs and fish-like robots [13,14,19]. Following these examples, we conjecture that added mass effects can be disregarded in this paper. The control-oriented model without added mass effects is obtained from (2) by setting $\mu_p = 0$. The generalised mass then reduces to $\widetilde{m} = m$.

In order to verify that the control-oriented model is an adequate representation of a USR, we present an extensive simulation study in Sec. V, where the control-oriented model is compared to a first-principle model. To verify the particular assumption that added mass effects can be disregarded, simulation results are compared with and without taking the added mass terms into account. Some preliminary results are listed in Tab. I, which shows the relative error of the relative forward velocity $v_{t,\mathrm{rel}}$ for different gaits. It was obtained from the simulation results by taking the mean of the forward velocity of both cases, subtracting the velocity without added mass from the velocity with added mass. The result was normalised by dividing by the velocity with added mass. It can be concluded from the table that, as far as forward velocity goes, disregarding added mass effects is a reasonable assumption. In Sec. V, more extensive simulation results will be presented, also taking into account normal velocity, orientation, and turning motion.

With the additional simplifications presented in the previous paragraphs, the simplified control-oriented model is

$$\dot{\boldsymbol{\phi}} = \mathbf{v}_\phi, \tag{6a}$$

$$\dot{\theta} = v_\theta, \tag{6b}$$

$$\dot{p}_x = v_t \cos\theta - v_n \sin\theta, \tag{6c}$$

$$\dot{p}_y = v_t \sin\theta + v_n \cos\theta, \tag{6d}$$

$$\boldsymbol{\mathcal{M}}\dot{\mathbf{v}}_\phi = -\boldsymbol{\mathcal{D}}\mathbf{v}_\phi - \boldsymbol{\mathcal{K}}(\mathbf{v})\boldsymbol{\phi} + \mathbf{D}\mathbf{D}^T\mathbf{u}, \tag{6e}$$

$$\dot{v}_\theta = -\lambda_1 v_\theta + \tfrac{\lambda_2}{N-1} v_{t,\mathrm{rel}} \bar{\mathbf{e}}^T \boldsymbol{\phi}, \tag{6f}$$

$$\dot{v}_t = -\tfrac{c_t}{m} v_{t,\mathrm{rel}} + \tfrac{2c_p}{Nm} \bar{\mathbf{e}}^T \boldsymbol{\phi} v_{n,\mathrm{rel}} - \tfrac{c_p}{Nm} \boldsymbol{\phi}^T \mathbf{A}\bar{\mathbf{D}}\mathbf{v}_\phi, \tag{6g}$$

$$\dot{v}_n = \tfrac{2c_p}{Nm} \bar{\mathbf{e}}^T \boldsymbol{\phi} v_{t,\mathrm{rel}} - \tfrac{c_n}{m} v_{n,\mathrm{rel}}, \tag{6h}$$

where the matrices $\boldsymbol{\mathcal{M}}(\boldsymbol{\phi}), \boldsymbol{\mathcal{D}}(\boldsymbol{\phi}), \boldsymbol{\mathcal{K}}(\boldsymbol{\phi}, \mathbf{v})$ reduce to $\boldsymbol{\mathcal{M}} = m\mathbf{I}_{N-1}$, $\boldsymbol{\mathcal{D}} = c_n \mathbf{I}_{N-1}$, and $\boldsymbol{\mathcal{K}}(\mathbf{v}) = -c_p v_{t,\mathrm{rel}} \mathbf{A}\mathbf{D}^T$.

Note that this model has the same structure as the one for ground robots in [9,16]. The friction coefficients of the ground model play the same role as the drag parameters of the USR, and the control-oriented model in [9] thus is a special case of this model. The new feature of the model presented here with respect to one in [9,16] is its ability to take into account disturbances from ocean currents.

3) A generalised gait: In order to achieve forward propulsion, the joints of the robot are controlled such that they track a sinusoidal wave propagating through the body from head to tail. For the derivation of the control-oriented model in [11], the amplitude of that wave was assumed to be constant, resulting in a gait called lateral undulation. In this paper, the model is extended to hold for a general sinusoidal gait from [15], yielding the following reference signal for the joints:

$$\phi_{i,\mathrm{ref}}(t) = \alpha g(i) \sin\left(\omega t + (i-1)\delta\right) + \phi_0. \tag{7}$$

Here, α is the maximum amplitude of the joint oscillation, ω is the frequency, δ is the phase shift between the single links that defines the wave length, and ϕ_0 is a constant offset that induces turning motion. The function $g : \mathbb{R} \mapsto [0, 1]$ scales the amplitude of the single joints ϕ_i, and can therefore be used to vary the wave amplitude along the body. In particular, the gait *lateral undulation*, which is mainly observed for ground snakes [9], can be described by choosing $g(i) = 1$, and *eel-like motion* can be achieved by the choice $g(i) = \frac{N-i}{N+1}$ [2]. In fact, eels have been observed to undulate with an increasing amplitude in water, while mimicking lateral undulation on land [20].

When applying the reference signal (7) to the simplified model with translational joints, the joints have to be controlled to oscillate with an amplitude α that is given in a unit of length. For a physical robot on the other hand, the joints are revolute and controlled to move with an amplitude α, which is an angle. In order to allow a comparison between both cases, a mapping of these amplitudes has to be found. In [11], the control-oriented model was restricted to move with the gait lateral undulation and the phase shift δ was assumed to be chosen in a way such that the wave length of the gait equals the body length $\delta = \frac{2\pi}{N-1}$. These assumptions are restrictive, but they allowed to derive an analytical relation between the translational and the revolute amplitude by interpreting the translational link motion as a projection of the revolute link motion onto the subspace orthogonal to the orientation $\bar{\theta}$ of the robot. Details can be found in [11].

For eel-like motion on the other hand, an analogue relation cannot be found due to the lack of nose-tail symmetry in the gait. However, in [10] it was shown that eel-like motion of a complex model can be approximated by the control-oriented model by simply mapping the amplitudes by trial and error. We therefore conjecture that the control-oriented model is able to approximate the behaviour of the complex model for eel-like motion also by using the analytical mapping for the joint amplitudes from [11]. An extensive simulation study, where both models are compared, will be presented in Sec. V.

III. Controller design

The feedback linearising control law

$$\mathbf{u} = (\mathbf{D}\mathbf{D}^T)^{-1}\Big[\boldsymbol{\mathcal{M}}\bar{\mathbf{u}} + \boldsymbol{\mathcal{D}}\dot{\boldsymbol{\phi}} + \boldsymbol{\mathcal{K}}(\mathbf{v})\boldsymbol{\phi}\Big] \tag{8}$$

is applied to the USR. It transforms the joint dynamics (6e) to $\dot{\mathbf{v}}_\phi = \bar{\mathbf{u}}$ such that the new input $\bar{\mathbf{u}} = [\bar{u}_1 \cdots \bar{u}_{N-1}]^T \in \mathbb{R}^{N-1}$ directly controls the joint coordinates [11].

As proposed in [15], the control input $\bar{\mathbf{u}}$ is chosen as

$$\bar{\mathbf{u}} = \ddot{\boldsymbol{\phi}}_{\mathrm{ref}} + k_d(\dot{\boldsymbol{\phi}}_{\mathrm{ref}} - \dot{\boldsymbol{\phi}}) + k_p(\boldsymbol{\phi}_{\mathrm{ref}} - \boldsymbol{\phi}), \tag{9}$$

where k_d and k_p are positive control gains, and the derivatives of $\phi_{i,\mathrm{ref}}(t)$ are given by

$$\begin{aligned} \dot{\phi}_{i,\mathrm{ref}}(t) &= \alpha g(i)\omega\cos\left(\omega t + (i-1)\delta\right), \\ \ddot{\phi}_{i,\mathrm{ref}}(t) &= -\alpha g(i)\omega^2\sin\left(\omega t + (i-1)\delta\right), \end{aligned} \tag{10}$$

under the assumption that ϕ_0 is constant. With the control law (9), the dynamics of the joint errors $\tilde{\boldsymbol{\phi}} = \boldsymbol{\phi} - \boldsymbol{\phi}_{\mathrm{ref}}$ are

$$\ddot{\tilde{\boldsymbol{\phi}}} + k_d\dot{\tilde{\boldsymbol{\phi}}} + k_p\tilde{\boldsymbol{\phi}} = 0, \tag{11}$$

which is uniformly globally exponentially stable (UGES).

Remark 2: Note that disregarding added mass effects and setting $\widehat{c}_n$ to zero is not a condition for UGES. The same stability property holds when the presented controller is applied to the model in (2).

IV. The velocity dynamics

In this section, the velocity dynamics of the simplified model (6) whose joints follow the reference signal (7) will be analysed using averaging theory. At first, the model will be reduced to include only the relevant dynamics, and then be transformed to an averaged model. Using the new model of the averaged velocities, the steady state behaviour of the robot will be analysed and relationships between the gait parameters and the relative forward velocity will be derived.

A. A model of the velocity dynamics

Similar to the analyses in [9,15], the state vector for the velocity dynamics is defined as

$$\mathbf{v} = [v_t \; v_n \; v_\theta]^T \in \mathbb{R}^3. \tag{12}$$

From Eqs. (6f–6h) the velocity dynamics is

$$\dot{\mathbf{v}} = \begin{bmatrix} -\frac{c_t}{m}v_{t,\mathrm{rel}} + \frac{2c_p}{Nm}v_{n,\mathrm{rel}}f_1(\omega t) - \frac{c_p}{Nm}f_2(\omega t) \\ -\frac{c_n}{m}v_{n,\mathrm{rel}} + \frac{2c_p}{Nm}v_{t,\mathrm{rel}}f_1(\omega t) \\ -\lambda_1 v_\theta + \frac{\lambda_2}{N-1}v_{t,\mathrm{rel}}f_1(\omega t) \end{bmatrix} = \mathbf{f}(t,\mathbf{v}) \tag{13}$$

with

$$f_1(\omega t) = (N-1)\phi_0 + \sum_{i=1}^{N-1}\alpha g(i)\sin(\omega t + (i-1)\delta), \tag{14a}$$

$$\begin{aligned} f_2(\omega t) = \sum_{i=1}^{N-1}\sum_{j=1}^{N-1} a_{ij}\big[&\phi_0\alpha g(j)\omega\cos(\omega t + (j-1)\delta) \\ &+\alpha^2 g(i)g(j)\omega\sin(\omega t + (i-1)\delta)\cos(\omega t + (j-1)\delta)\big], \end{aligned} \tag{14b}$$

and a_{ij} denoting element (i,j) of the matrix $\mathbf{A}\bar{\mathbf{D}}$.

B. A model of the averaged velocity dynamics

In order to apply averaging to the model of the velocity dynamics, (13) needs to be transformed to the standard form $\frac{\mathrm{d}\mathbf{v}}{\mathrm{d}\tau} = \epsilon\mathbf{f}(\tau,\mathbf{v})$ (cf. Chap. 10.4, [21]). This is achieved by the choice $\tau = \omega t$, yielding $\frac{\mathrm{d}}{\mathrm{d}t} = \omega\frac{\mathrm{d}}{\mathrm{d}\tau}$ and $\epsilon = \frac{1}{\omega}$. The resulting model is 2π-periodic in τ and the averaged system is

$$\tfrac{\mathrm{d}\mathbf{v}_{\mathrm{av}}}{\mathrm{d}\tau} = \epsilon\tfrac{1}{2\pi}\int_0^{2\pi}\mathbf{f}(\tau,\mathbf{v})\mathrm{d}\tau. \tag{15}$$

By solving the integrals of $f_1(\tau)$ and $f_2(\tau)$,

$$\int_0^{2\pi} f_1(\tau)\mathrm{d}\tau = 2\pi(N-1)\phi_0, \tag{16a}$$

$$\int_0^{2\pi} f_2(\tau)\mathrm{d}\tau = -\pi\underbrace{\alpha^2\omega}_{k_{\alpha\omega}}\underbrace{\sum_{i=1}^{N-1}\sum_{j=1}^{N-1} a_{ij}g(i)g(j)\sin((j-i)\delta)}_{k_\delta}, \tag{16b}$$

the averaged model is obtained:

$$\begin{aligned} \tfrac{\mathrm{d}\mathbf{v}_{\mathrm{av}}}{\mathrm{d}\tau} &= \epsilon\begin{bmatrix} -\frac{c_t}{m}v_{t,\mathrm{rel}} + \frac{2c_p(N-1)}{Nm}\phi_0 v_{n,\mathrm{rel}} + \frac{c_p}{2Nm}k_{\alpha\omega}k_\delta \\ -\frac{c_n}{m}v_{n,\mathrm{rel}} + \frac{2c_p(N-1)}{Nm}\phi_0 v_{t,\mathrm{rel}} \\ -\lambda_1 v_\theta + \lambda_2\phi_0 v_{t,\mathrm{rel}} \end{bmatrix} \\ &= \epsilon\big(\boldsymbol{\mathcal{A}}\mathbf{v} + \boldsymbol{\mathcal{B}}\big), \end{aligned} \tag{17}$$

$$\text{with } \boldsymbol{\mathcal{A}}(\phi_0) = \begin{bmatrix} -\frac{c_t}{m} & \frac{2c_p(N-1)}{Nm}\phi_0 & 0 \\ \frac{2c_p(N-1)}{Nm}\phi_0 & -\frac{c_n}{m} & 0 \\ \lambda_2\phi_0 & 0 & -\lambda_1 \end{bmatrix},$$

$$\boldsymbol{\mathcal{B}}(\phi_0) = \begin{bmatrix} \frac{c_p}{2Nm}k_{\alpha\omega}k_\delta \\ 0 \\ 0 \end{bmatrix} - \boldsymbol{\mathcal{A}}(\phi_0)\begin{bmatrix} V_t \\ V_n \\ 0 \end{bmatrix}. \tag{18}$$

The final version of the averaged model of the velocity dynamics is obtained by changing the time-scale back to t:

$$\dot{\mathbf{v}}_{\mathrm{av}} = \tfrac{\mathrm{d}\mathbf{v}_{\mathrm{av}}}{\mathrm{d}t} = \tfrac{1}{\epsilon}\tfrac{\mathrm{d}\mathbf{v}_{\mathrm{av}}}{\mathrm{d}\tau} = \boldsymbol{\mathcal{A}}\mathbf{v} + \boldsymbol{\mathcal{B}}. \tag{19}$$

The averaged model is a linear system that is characterised by the gait parameters and the velocity of the ocean current.

Remark 3: Due to the similar structure of the systems, the dynamic matrix of the averaged model (19) has the same structure as the one of a ground robot in [9]. The constant offset $\boldsymbol{\mathcal{B}}$, however, now includes the velocity of the current.

C. The averaged velocity dynamics in steady state

Similar to the procedure in [9,12] and [15], the offset $\boldsymbol{\mathcal{B}}$ is removed by the transformation $\mathbf{z} = \mathbf{v}_{\mathrm{av}} + \boldsymbol{\mathcal{A}}^{-1}\boldsymbol{\mathcal{B}}$ in order to analyse the stability of the averaged model:

$$\dot{\mathbf{z}} = \dot{\mathbf{v}}_{\mathrm{av}} = \boldsymbol{\mathcal{A}}(\mathbf{z} - \boldsymbol{\mathcal{A}}^{-1}\boldsymbol{\mathcal{B}}) + \boldsymbol{\mathcal{B}} = \boldsymbol{\mathcal{A}}\mathbf{z}. \tag{20}$$

In order to determine the stability properties of this linear system, the eigenvalues of $\boldsymbol{\mathcal{A}}$ are computed as

$$\text{eig}(\boldsymbol{\mathcal{A}}) = \begin{bmatrix} -\lambda_1 \\ -\frac{c_n+c_t}{2m} - \frac{\sqrt{(c_nN-c_tN)^2+(4(N-1)c_p\phi_0)^2}}{2Nm} \\ -\frac{c_n+c_t}{2m} + \frac{\sqrt{(c_nN-c_tN)^2+(4(N-1)c_p\phi_0)^2}}{2Nm} \end{bmatrix}. \quad (21)$$

Note that, even though the snake robot is now exposed to ocean currents, the eigenvalues are the same as for ground robots (cf. Eq. (7.24) in [9]). It can easily be verified that all eigenvalues in (21) are negative if

$$|\phi_0| < \frac{N}{2(N-1)} \frac{\sqrt{c_n c_t}}{c_p}, \quad (22)$$

a condition which implies that the equilibrium $\mathbf{z} = 0$ is globally exponentially stable. The constraint (22) on the offset ϕ_0 indicates that modelling the joints as translational rather than revolute is restricted to a limited displacement.

Under the assumption that ϕ_0 is sufficiently small for (22) to hold, $\mathbf{v}_{\text{av}}$ will converge to the steady state velocity

$$\begin{aligned} \mathbf{v}^* &= -\boldsymbol{\mathcal{A}}^{-1}\boldsymbol{\mathcal{B}} = -\boldsymbol{\mathcal{A}}^{-1} \begin{bmatrix} \frac{c_p}{2Nm} k_{\alpha\omega} k_\delta \\ 0 \\ 0 \end{bmatrix} + \begin{bmatrix} V_t \\ V_n \\ 0 \end{bmatrix}, \\ &= k_{\alpha\omega} k_\delta \begin{bmatrix} \frac{Nc_nc_p}{2(c_nc_tN^2-4(N-1)^2c_p^2\phi_0^2)} \\ \frac{c_p^2\phi_0(N-1)}{c_nc_tN^2-4(N-1)^2c_p^2\phi_0^2} \\ \frac{Nc_nc_p\lambda_2\phi_0}{2\lambda_1(c_nc_tN^2-4(N-1)^2c_p^2\phi_0^2)} \end{bmatrix} + \begin{bmatrix} V_t \\ V_n \\ 0 \end{bmatrix}. \end{aligned} \quad (23)$$

From (23) we see that the steady state velocity depends on the parameters of the gait, the drag parameters, the number of links, and the current velocity. The expression for the steady state velocity (23) includes the same parameters as for ground robots [9], to which the current velocities in the body frame are added. This was expected, since the averaged model was seen to have the same structure, with the additional capability of taking into account currents.

After establishing global exponential stability for the averaged velocity dynamics, the stability of the exact dynamics will be considered. According to Th. 10.4 in [21], it follows from the stability of the averaged dynamics that, for sufficiently small ϵ, the average velocity given by (23) approximates the exact velocity (13) for all time and with an error that is bounded. This means that, if ω is sufficiently large, the periodic time-varying velocity will remain close to the exponentially stable averaged velocity for all time.

Theorem 1: Consider a planar USR described by (6) controlled in accordance with a gait according to (7, 10) and the offset ϕ_0 satisfying (22). Then there exist $k > 0$, $\omega^* > 0$ such that the following holds for all $\omega > \omega^*$:

$$\|\mathbf{v}(t) - \mathbf{v}_{\text{av}}(t)\| \leq \tfrac{k}{\omega} \;\; \forall t > 0. \quad (24)$$

In addition, the averaged velocity $\mathbf{v}_{\text{av}}(t)$ converges exponentially to the steady-state velocity $\mathbf{v}^*$ in (23).

Remark 4: Note that the presence of constant irrotational currents does not influence the stability properties of the snake robot, since the eigenvalues (21) do not depend on the current. The current only moves the equilibrium of the velocity dynamics. Moreover, by subtracting the current velocities from both sides of (23), it can be shown that the *relative* velocities converge to the same value as the velocities of a ground robot [9].

D. Relationship between $v_{t,\text{rel}}$ and the gait parameters

With the averaged steady state velocity for a planar USR moving with a sinusoidal gait that was presented in the previous section, it becomes possible to analyse a scenario that is particularly interesting with respect to motion planning purposes: steady state motion with zero offset $\phi_0 = 0$, which will be shown to be motion in a straight line.

By inserting $\phi_0 = 0$ into (23) and subtracting the current velocities from both sides, the expression

$$\begin{bmatrix} v^*_{t,\text{rel}} \\ v^*_{n,\text{rel}} \\ v^*_\theta \end{bmatrix} = \begin{bmatrix} k_{\alpha\omega}k_\delta \frac{c_p}{2c_tN} \\ 0 \\ 0 \end{bmatrix} \quad (25)$$

is obtained. It can easily be seen that the relative velocity normal to the robot's orientation is zero, as is the rotational velocity. This means that the robot moves in a straight line, with its absolute normal velocity equal to the normal current velocity. For the forward velocity, the following property can be derived from (25), keeping in mind that $k_{\alpha\omega} = \alpha^2\omega$:

Corollary 1: Consider a planar USR described by (6) controlled in accordance with a gait according to (7, 10). For $\omega > \omega^*$ and sufficiently small ϕ_0 for (22) to hold, the averaged relative forward velocity of the robot will converge exponentially to $v^*_{t,\text{rel}}$, which is proportional to

- the squared amplitude of the joints, α^2
- the frequency of the gait, ω
- a function of the phase shift δ, which is given by

$$k_\delta = \sum_{i=1}^{N-1}\sum_{j=1}^{N-1} a_{ij} g(i) g(j) \sin((j-i)\delta). \quad (26)$$

This result extends the findings of previous studies: In [14], it was shown that the averaged forward dynamics of a three- and a five-link eel-like robot are captured by a function proportional to the squared amplitude, frequency, and a sum of sinusoidal functions. In [9], the special case of lateral undulation, yielding both $g(i) = g(j) = 1$, was investigated. As pointed out in [9], Cor. 1 provides a powerful tool for motion planning: an increase/decrease of the relative forward velocity can be invoked by using α or ω as a control input. Furthermore, the controller can be optimised by finding the optimal phase shift δ that maximises k_δ for the given number of links and choice of gait.

V. Simulation Study

In order to validate the control-oriented model proposed in Sec. II and the theoretical findings from the averaging analysis, extensive simulations have been carried out. This section summarises the results. At first the behaviour of the improved control-oriented model and a first-principle model is compared. In the second part, the averaged velocity dynamics is compared to the exact one, and finally, the relationship between the gait parameters and the relative forward velocity is investigated.

TABLE II

COMBINATIONS OF GAIT PARAMETERS

Case #	1	2	3	4	5	6	7	8	9
$\theta_{\max}$	$10°$	$20°$	$30°$	$20°$	$20°$	$20°$	$20°$	$20°$	$20°$
α_{comp}	$6.84°$	$13.7°$	$20.5°$	$13.7°$	$13.7°$	$13.7°$	$12.0°$	$16.9°$	$20.0°$
α_{simp}	$2.94\,\text{cm}$	$5.79\,\text{cm}$	$8.46\,\text{cm}$	$5.79\,\text{cm}$	$5.79\,\text{cm}$	$5.79\,\text{cm}$	$5.87\,\text{cm}$	$5.58\,\text{cm}$	$5.33\,\text{cm}$
ω	$120°/\text{s}$	$120°/\text{s}$	$120°/\text{s}$	$60°/\text{s}$	$80°/\text{s}$	$100°/\text{s}$	$120°/\text{s}$	$120°/\text{s}$	$120°/\text{s}$
δ	$40°$	$40°$	$40°$	$40°$	$40°$	$40°$	$35°$	$50°$	$60°$

TABLE III

MODEL PARAMETERS AND CONTROL GAINS

l	0.09 m	m	1.56 kg	$\widetilde{m}$	4.12 kg	μ_p	7.13 $\frac{\text{kg}}{\text{m}}$
c_n	17.3	c_t	4.45	c_p	35.8	$\widehat{c}_n$	0
λ_1	6	λ_2	120	k_p	200	k_d	50

A. Comparison of different USR models

1) Simulation set-up: As a reference to compare the behaviour of the control-oriented model both with and without added-mass effects, a first-principle model of a USR that was presented in [2] was used. The model parameters were chosen in order to resemble the parameters that were found in an experimental parameter identification of a physical robot in [18], and are summarised in Tab. III. The gains that were chosen for the control system can also be found in Tab. III. The mass of each link was set to $m = 1.56$ kg, in order to guarantee neutral buoyancy. The turning coefficients λ_1, λ_2 were found by tuning the behaviour of a lateral undulating 10-linked USR with the gait parameters according to Case 2 in Tab. II. All models were implemented and simulated in *Matlab R2014b*. The dynamics of the models was calculated by the *ode23tb* solver with a relative and absolute error tolerance of 10^{-4}. All initial values were set to the origin. The simulations were carried out for USRs with $n = 7, 10, 19$ links, respectively. Nine different combinations of gait parameters were considered, they are listed in Tab. II. The amplitude α was derived from the maximal link angle $\theta_{\max}$ by the formulas in [11]. They are presented in Tab. II as α_{comp} for the first-principle model and α_{simp} for the control-oriented one. Each case was simulated for both lateral undulation and eel-like motion.

At first, straight motion was investigated. All parameter cases and models were simulated with $\phi_0 = 0$ while the current velocity was set to zero. With the simulation results, current velocities for testing the model behaviour in the presence of currents could be determined: the average x-velocity $\bar{\dot{p}}_x$ of the first-principle model was computed for each of the simulated scenarios and the current velocity was then chosen as $0.7\bar{\dot{p}}_x$ for each of the scenarios. The angle of attack was set to $30°$. By this choice, the USR was experiencing a significant disturbance, but still able to compensate for it with the forward velocity. All simulations were then run again with the current.

In a second step, a scenario including turning motion was simulated. In order to do so, the joint offset ϕ_0 was set to $\frac{\alpha}{6}$ in the time interval $t \in [40\text{s}, 70\text{s}]$, to $-\frac{\alpha}{6}$ in $t \in [130\text{s}, 160\text{s}]$, and to zero elsewhere. This scenario was simulated with and without current, too.

2) Simulation results: Straight motion: The simulations showed that the *qualitative* behaviour of the USR of the control-oriented model is in good accordance with the first-principle model. Added mass effects turned out to have very little effect on the control-oriented model, and the presence or absence of the current did not affect the similarity between the models. The *quantitative* similarity between the models, however, strongly depends on the assumptions concerning the link angles, $|\theta_i| < 20°$, and the phase shift $\delta = \frac{2\pi}{N-1}$.

For lateral undulation, the control-oriented model tends to overestimate the velocity for an increasing α. This agrees with Ass. 1 of small link angles. For eel-like motion, this effect was not observed, as can be seen in Fig. 3(a), where a good *quantitative* similarity between the models is achieved even for a relatively large α. This can be explained by the fact that for eel-like motion, only the tail link is oscillating with the full amplitude, whereas for lateral undulation, every single link contributes with a higher amplitude than assumed. The variation of the frequency ω did not have an effect on the similarity of both models. Changing the offset δ or the number of links had the biggest influence on the similarity between the models for both gaits. Fig. 3(b) shows the same scenario as Fig. 3(a), only that δ was changed from $40°$ to $60°$. For a robot with $n = 7$ links, the phase shift $\delta = 50°$ led to the best *quantitative* approximation for eel-like motion, as can be seen in Fig. 3(c). Fig. 3 shows that the assumption $\delta = \frac{2\pi}{N-1}$ is important for a good *quantitative* approximation.

3) Simulation results: Turning motion: Just like in the straight motion scenario, neither added mass effects, nor the choice of ω, nor the current had an effect on the similarity between the models. In addition, the choice of α did not have an influence on the turning performance, only on the velocity. In order to achieve a good *quantitative* approximation, the choice of δ and n, on the other hand, had a large influence. Fig. 4(a) presents the results for a 10-linked USR moving in the presence of a current with lateral undulation according to Case 2 in Tab. II. In Fig. 4(b), the analogous scenario is shown for eel-like motion. A good *quantitative* approximation can be observed for eel-like motion. The velocity is slightly overestimated by the lateral undulating model, while the orientation still shows good accordance. The performance of the lateral undulating 7-linked robot in Fig. 4(c) stands in contrast to the previous results. Even though there is a very good *quantitative* approximation of the velocity for $\delta = 60°$, the turning behaviour is only in *qualitative* accordance. This suggests that the turning parameters λ_i, that have been tuned for Case 2, depend on δ and n.

B. Comparison of the original and the averaged velocity

In order to investigate the performance of the averaged velocity dynamics, the same scenarios that were described

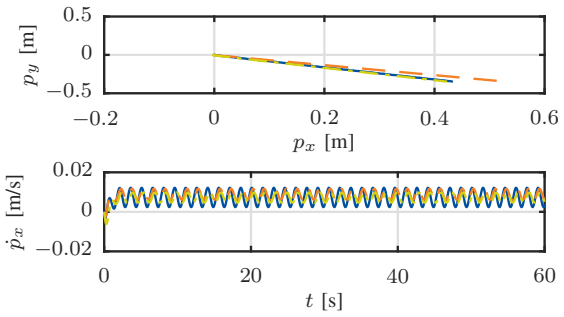

(a) $n = 10$ links, eel-like motion according to Case 2

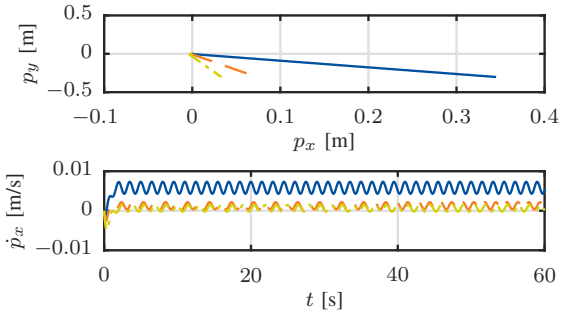

(b) $n = 10$ links, eel-like motion according to Case 9

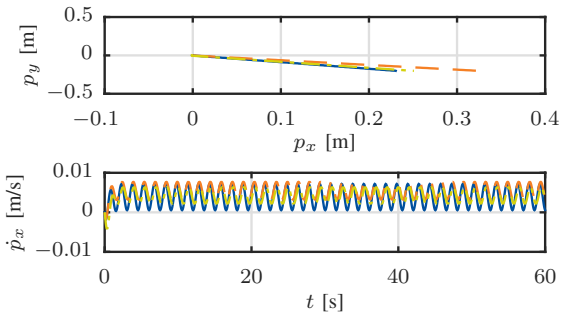

(c) $n = 7$ links, eel-like motion according to Case 8

First-principle model
Control-oriented model with added mass effects
Control-oriented model without added mass effects

Fig. 3. Comparison of straight motion

in Sec. V-A.1 were simulated with the averaged model (19). The results showed excellent accordance with the results of the control-oriented model (6). An example is presented in Fig. 5, where the velocity dynamics of both the control-oriented model and the averaged model are plotted for lateral undulation with 10 links and the gait parameters of Case 2.

C. Relationship between the gait parameters and $v_{t,\mathrm{rel}}$

From all the simulations that were described in Sec. V-A.1, several cases of the straight motion scenarios with current were evaluated in order to validate the relationships between the relative forward velocity and the gait parameters α and ω, that were derived in Sec. IV-D. The evaluated cases were Cases 1-3 in Tab. II in order to check the dependency on α, and Cases 4-6 and 2 for ω.

Fig. 6 shows the relative forward velocities that were obtained for the different α. In the same manner, the relative forward velocities for the different choices of ω are plotted

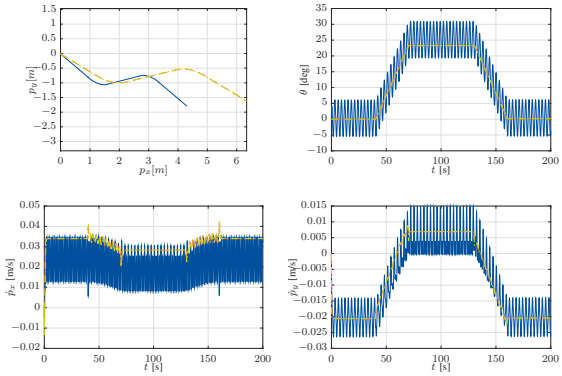

(a) $n = 10$ links, lateral undulation according to Case 2

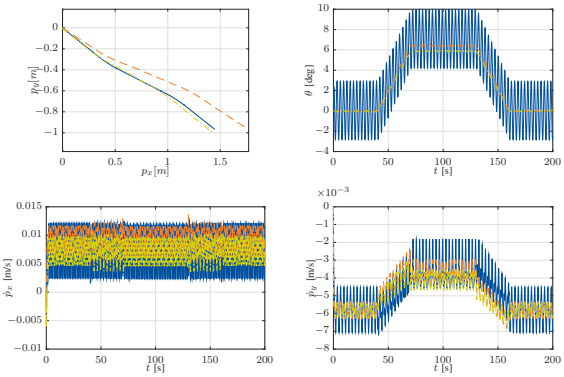

(b) $n = 10$ links, eel-like motion according to Case 2

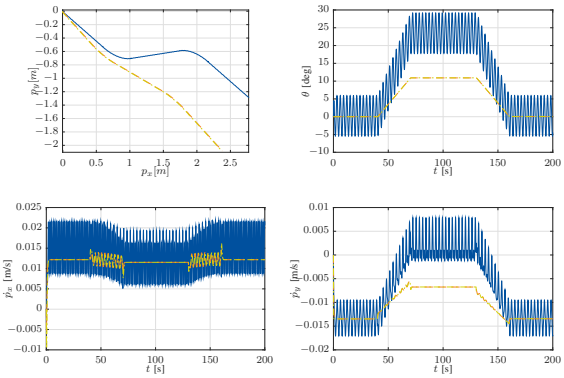

(c) $n = 7$ links, lateral undulation according to Case 9

First-principle model
Control-oriented model with added mass effects
Control-oriented model without added mass effects

Fig. 4. Comparison of turning motion

in Fig. 7, and there is clearly a linear relationship.

VI. Conclusions and Future Work

In this paper, an analysis of planar underwater snake robot locomotion in the presence of ocean currents was presented. The USR was assumed to be neutrally buoyant, fully submerged, and move with a planar sinusoidal gait and limited link angles. An existing, control-oriented model was further simplified and extended to general sinusoidal gaits to serve as a basis for the analysis. The averaged velocity

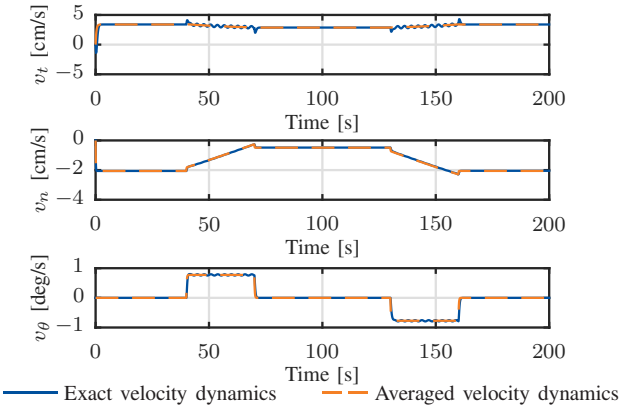

Fig. 5. The averaged and the exact velocity dynamics

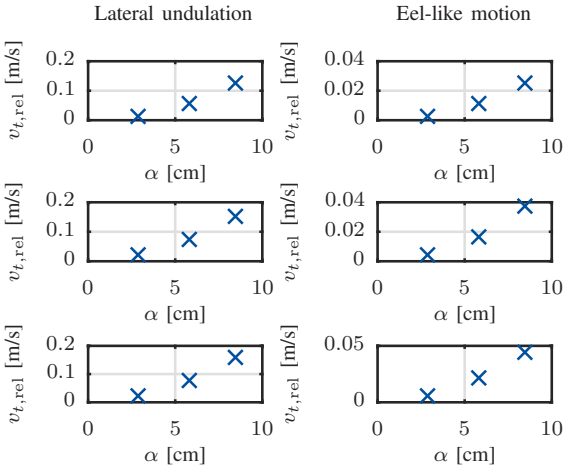

Fig. 6. The relationship between $v_{t,\mathrm{rel}}$ and α for $n = 7$ (top), $n = 10$ (center), and $n = 19$ (bottom) links

dynamics of the underwater snake robot were derived using averaging theory. It was proven that the averaged velocity converges exponentially to an equilibrium, and an analytical expression for calculating the relative forward velocity of the robot in steady state was presented. In particular, it was shown that the relative forward velocity is 1) proportional to the square of the amplitude of the sinusoidal gait, α^2, 2) proportional to the frequency of the sinusoidal gait, ω, and 3) a function of the phase shift δ of the gait. Extensive simulations were carried out that qualitatively validated the proposed modelling approach and supported the theoretical findings of the locomotion analysis.

In future work, the findings of this study will be applied for controller design, guidance, and motion planning algorithms for USRs. An extension of the results to hold for arbitrary motion in three dimensions will be pursued. Experiments in order to validate the theoretical findings will be conducted.

References

[1] M. Porez, F. Boyer, and A. J. Ijspeert, "Improved lighthill fish swimming model for bio-inspired robots: Modeling, computational aspects and experimental comparisons," *Int. J. Robot. Res.*, vol. 33, no. 10, pp. 1322–1341, 2014.

[2] E. Kelasidi, K. Y. Pettersen, J. T. Gravdahl, and P. Liljebäck, "Modeling of underwater snake robots," in *Proc. IEEE Int. Conf. Robotics and Automation*, Hong Kong, China, May, Jun. 2014.

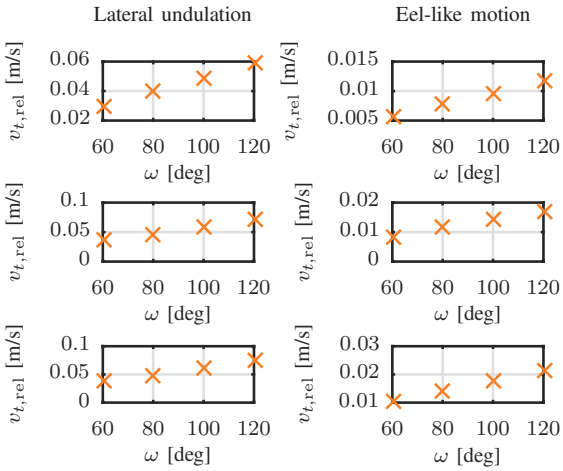

Fig. 7. The relationship between $v_{t,\mathrm{rel}}$ and ω for $n = 7$ (top), $n = 10$ (center), and $n = 19$ (bottom) links

[3] J. Gray, "Studies in animal locomotion I. the movement of fish with special reference to the eel," *J. Exp. Biol.*, vol. 10, no. 1, pp. 88–104, 1933.

[4] ——, "The mechanism of locomotion in snakes," *J. Exp. Biol.*, vol. 23, no. 2, pp. 101–120, 1946.

[5] S. Hirose, *Biologically Inspired Robots: Snake-Like Locomotors and Manipulators*. Oxford: Oxford University Press, 1993.

[6] H. Yamada, S. Chigisaki, M. Mori, K. Takita, K. Ogami, and S. Hirose, "Development of amphibious snake-like robot ACM-R5," in *Proc. 36th Int. Symp. Robotics*, Tokyo, 2005.

[7] P. Liljebäck, Ø. Stavdahl, K. Pettersen, and J. Gravdahl, "Mamba - A waterproof snake robot with tactile sensing," in *Proc. IEEE/RSJ Int. Conf. Intelligent Robots and Systems*, Chicago, IL, Sep. 2014.

[8] K. Mclsaac and J. Ostrowski, "A geometric approach to anguilliform locomotion: modelling of an underwater eel robot," in *Proc. IEEE Int. Conf. Robotics and Automation*, Detroit, MI, May 1999.

[9] P. Liljebäck, K. Y. Pettersen, Ø. Stavdahl, and J. T. Gravdahl, *Snake Robots: Modelling, Mechatronics, and Control*, ser. Advances in Industrial Control. Springer London, 2012.

[10] E. Kelasidi, K. Y. Pettersen, and J. T. Gravdahl, "A control-oriented model of underwater snake robots," in *Proc. IEEE Int. Conf. Robotics and Biomimetics*, Bali, ID, Dec. 2014.

[11] A. M. Kohl, E. Kelasidi, K. Y. Pettersen, and J. T. Gravdahl, "A control-oriented model of underwater snake robots exposed to currents," in *Proc. IEEE Multi-Conf. Systems and Control*, Sydney, Australia, Sep. 2015.

[12] P. Liljebäck, K. Y. Pettersen, Ø. Stavdahl, and J. T. Gravdahl, "Stability analysis of snake robot locomotion based on averaging theory," in *Proc. IEEE Conf. Decision and Control*, Atlanta, 2010.

[13] J. Wang, S. Chen, and X. Tan, "Control-oriented averaging of tail-actuated robotic fish dynamics," in *Proc. American Control Conference*, Washington, DC, June 2013.

[14] K. A. McIsaac and J. P. Ostrowski, "Motion planning for anguilliform locomotion," *IEEE Trans. Robot. Autom.*, vol. 19, no. 4, pp. 637–652, 2003.

[15] E. Kelasidi, K. Y. Pettersen, and J. T. Gravdahl, "Stability analysis of underwater snake robot locomotion based on averaging theory," in *Proc. IEEE Int. Conf. Robotics and Biomimetics*, Bali, ID, Dec. 2014.

[16] P. Liljebäck, K. Y. Pettersen, Ø. Stavdahl, and J. T. Gravdahl, "A simplified model of planar snake robot locomotion," in *Proc. IEEE/RSJ Int. Conf. Intelligent Robots and Systems*, Taipei, Taiwan, Oct. 2010.

[17] E. Kelasidi, K. Y. Pettersen, and J. T. Gravdahl, "Modeling of underwater snake robots in a vertical plane in 3D," in *Proc. IEEE/RSJ Int. Conf. Intelligent Robots and Systems*, Chicago, 2014.

[18] E. Kelasidi, P. Liljebäck, K. Y. Pettersen, and J. T. Gravdahl, "Biologically inspired swimming snake robots: Modeling, control and experimental investigation," conditionally accepted. *IEEE Robotics and Automation Magazine* 2015.

[19] J. E. Colgate and K. M. Lynch, "Mechanics and control of swimming: A review," *IEEE J. Ocean. Eng.*, vol. 29, no. 3, pp. 660–673, 2004.

[20] G. B. Gillis, "Environmetal effects on undulatory locomotion in the American eel *Anguilla Rostrata*: Kinematics in water and on land," *J. Exp. Biol.*, vol. 201, no. 7, pp. 949–961, 1998.

[21] H. Khalil, *Nonlinear Systems*, 3rd ed. Prentice Hall, 2002.